Why Nanoprojectiles Work Differently than Macroimpactors: The Role of Plastic Flow

Christian Anders,[1] Eduardo M. Bringa,[2] Gerolf Ziegenhain,[1] Giles A. Graham,[3] J. Freddy Hansen,[4] Nigel Park,[5] Nick E. Teslich,[4] and Herbert M. Urbassek[1,*]

[1]*Fachbereich Physik und Forschungszentrum OPTIMAS, Universität Kaiserslautern, Erwin-Schrödinger-Straße, D-67663 Kaiserslautern, Germany*

[2]*CONICET and Instituto de Ciencias Básicas, Universidad Nacional de Cuyo, Mendoza, 5500 Argentina*

[3]*Mineralogy Department, The Natural History Museum, London SW7 5BD, United Kingdom*

[4]*Lawrence Livermore National Laboratory, Livermore, California 94550, USA*

[5]*AWE, Plc Aldermaston, Reading, United Kingdom*

(Received 5 April 2011; revised manuscript received 11 November 2011; published 11 January 2012)

Atomistic simulation data on crater formation due to the hypervelocity impact of nanoprojectiles of up to 55 nm diameter and with targets containing up to 1.1×10^{10} atoms are compared to available experimental data on μm-, mm-, and cm-sized projectiles. We show that previous scaling laws do not hold in the nanoregime and outline the reasons: within our simulations we observe that the cratering mechanism changes, going from the smallest to the largest simulated scales, from an evaporative regime to a regime where melt and plastic flow dominate, as is expected in larger microscale experiments. The importance of the strain-rate dependence of strength and of dislocation production and motion are discussed.

DOI: 10.1103/PhysRevLett.108.027601 PACS numbers: 79.20.Ap, 61.80.Lj, 96.25.Pq, 96.50.Dj

Crater formation by the impact of projectiles of various kinds—such as meteorites [1] or dust particles [2]—is of foremost interest to space science and to various technological applications such as surface nanostructuring [3]. Up to now the understanding of crater formation hinged mostly on the analysis of experiments and hydrocode simulations. Recently it became apparent that craters formed by nm-sized objects may exhibit different features [2] than their macroscopic variants. Here we present large-scale atomistic simulations of hypervelocity impact that span 5 orders of magnitude in projectile size, and targets including up to 11×10^9 atoms, and compare them with available experimental data allowing us to observe and interpret a *nonlinear* behavior of the crater volume with the impact energy, unlike the *linear* behavior generally assumed, which is correct only when considering narrow projectile size ranges. We explain the transition from nano- to macroregimes by the emergence of melt and plastic flow.

A linear dependence is found in experiments of μm- and mm-sized metal dust particles or bullets on various materials; hydrocode simulations typically do not include an intrinsic length scale, and also display this linear behavior. Experiments [3] and molecular-dynamics simulations of cluster impacts [4,5] have found this linear scaling. However, the question remains whether this extensive set of results from nanoscopic to macroscopic impacts can be understood within the same framework.

We scale the total projectile energy E with the target cohesive energy U, since in previous work [6] we found that crater volumes—both in metals and van der Waals bonded materials—scale well with E/U. Indeed Fig. 1 shows crater volume V vs scaled total cluster energy E/U for simulational and experimental data. It is essential to note that, although the scaling is linear at a given size scale above a threshold energy [5,6], there are discrepancies in between scales, pointing at a generally nonlinear dependence on E.

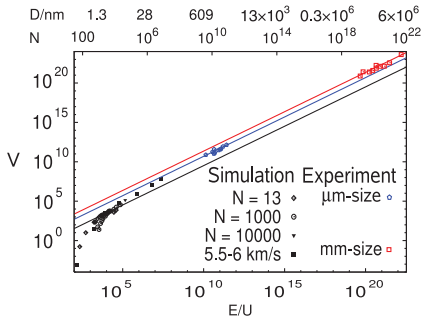

FIG. 1 (color). Synopsis of experimental and simulation data of dimensionless crater volumes V in a Cu target vs scaled impact energies E/U. The crater volume V is measured in dimensionless units as the number of atoms missing in the excavated crater below the initial surface plane (in agreement with the so-called *apparent* crater size used in the planetary-crater community [32]), and energy is scaled to the target cohesive energy U. Lines indicate a linear relationship, $V = aE/U$; Eq. (1). Experimental data taken from Refs. [33–35], see also additional material in the Supplemental Material [16]. Our simulation results have been taken for clusters of a fixed size $N = 13$, $N = 1000$, and $N = 10\,000$ with varying velocity, and for a fixed velocity $v = 5.5$ or 6 km/s for clusters with varying size, $N = 1 \times 10^3$–7.4×10^6. The upper abscissa gives cluster size N assuming Cu projectiles with 6 km/s. For Cu clusters, the diameter D depends on N as $D = N^{1/3} \times 0.28$ nm. We have observed similar behavior for other metallic targets and for van der Waals bonded targets [6,28], suggesting its universality.

To try to understand this transition from nano- to macroscales, we extend the simulations to include projectile sizes of up to several million atoms (which need targets of up to 11×10^9 atoms in our simulations), at about the limit of presentday computational possibilities [7]. In this regime, scaling becomes nonlinear [10] and moves towards the scaling appropriate for μm-sized projectiles. Two main reasons are operative to cause this change in behavior in our simulations. The first is the melt flow caused by the projectile which acts as a piston excavating the molten material, ejecting large liquid droplets, Fig. 2(a). Figure 3 shows an experimental secondary electron image of a crater in Al, with a structure that is evocative of a frozen melt flow. Melt flows are known to contribute to macroscopic crater formation [11,12], and are also observed in simulations of nanoimpacts [13,14]. The second new feature, which only shows up for projectile sizes exceeding ~5 nm, is the emergence of plastic flow, which becomes visible as dislocations in the target below the stopped projectile, Fig. 2(b). The consequences of dislocation build-up on the crater volume will be discussed below.

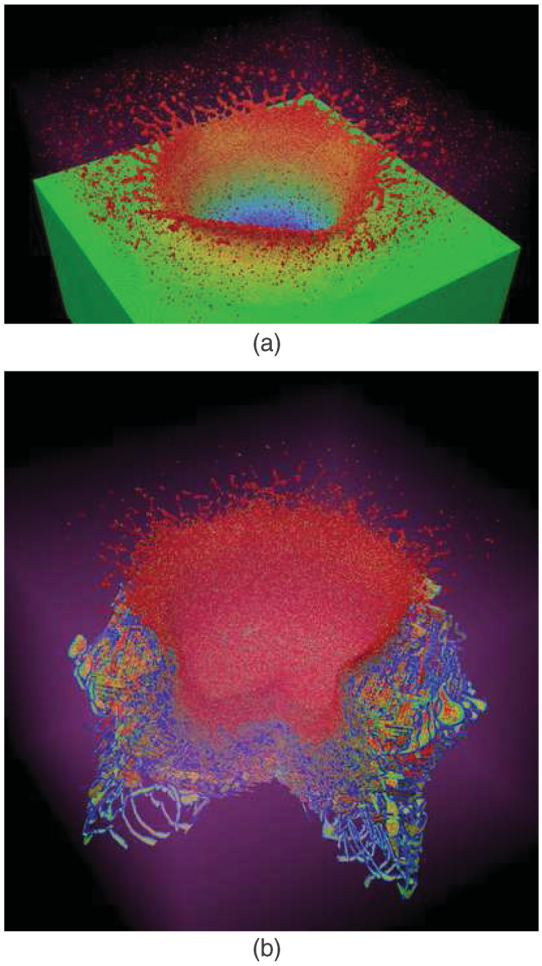

FIG. 2 (color). Molecular-dynamics simulation of a 40 nm diameter Cu sphere ($N = 2.8 \times 10^6$ atoms) impacting a single crystal Cu target with 5 km/s, at 21.5 ps after impact. Target size: 350×10^6 atoms. (a) Color code: velocity normal to target surface ($-2 \ldots +2$ km/s). Red: up; blue: down. (b) Same system, but showing only dislocations in the target. The anisotropy in the dislocation distribution is due to crystal structure.

Figure 1 demonstrates that—to a first approximation—the crater volume increases linearly with the total impact energy over more than 20 orders of magnitude. This simple correlation points at the fact that the underlying physics must be similarly simple in the energy and size regime investigated here. We model the apparently linear dependence via:

$$V = a\frac{E}{U}, \qquad E \gg E_{\mathrm{th}}. \tag{1}$$

We call the proportionality constant a the *cratering efficiency*. Here, E_{th} is a threshold energy; for energies $E < E_{\mathrm{th}}$ only a small crater is formed, whose size can be neglected here. V is a dimensionless volume, $V = V^*/\Omega$, where V^* is the volume of the crater and Ω the atomic volume under normal conditions. The influence of the threshold is seen only for the smallest impact energies for nanometric projectiles, as E_{th} increases only slowly with cluster size.

The simple proportionality in Eq. (1) describes well the data for projectiles of all sizes when they are considered separately. The cratering efficiency a assumes values of $a = 0.28$ for nanometric clusters (simulation results), $a = 5$ for μm-sized projectiles, and $a = 23$ for mm-sized projectiles; the accuracy in these values is about 5%. The slow change of crater efficiency a with cluster size is the central issue of this paper.

The cratering efficiency can be interpreted as follows: A cratering efficiency of $a = 1$ is indicative of a situation in which the entire projectile energy is used for bond breaking in the crater volume; the atomized material is then emitted.

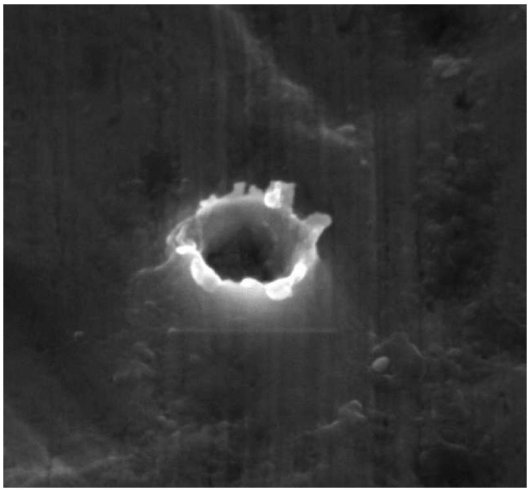

FIG. 3. Secondary electron image of an Al target from the Stardust mission, foil C054W, impacted by a cometary particle at a velocity ~6.1 km/s. The diameter of the impact feature is ~400 nm.

Large values of a give evidence that the majority of bonds are not broken during the crater evacuation process and hence collective effects become important.

The projectile energy is not only used for crater creation, but a large fraction is dissipated in the sample as heating, latent heat for phase change, shock waves, etc. For instance for clusters of up to few nm, the crater is carved mostly by evaporation of target atoms [6,15], but the efficiency is only ~0.3. For macroscopic impacts at moderate velocities of several km/s we can assume, following experimental and hydrocode studies, that the crater results from plastic flow and a significant amount of the energy will be dissipated as plastic heating. Based on our simulations and existing hydrocode simulations at larger scale, we can differentiate several regimes; for details see Supplemental Material [16]. For clusters of up to $\sim 10^3$ atoms, crater excavation is done by rapid evaporation in the ''threshold'' regime, with crater formation times (t_c) of a few ps, strain rates $\dot{\epsilon} \sim 10^{13}/\mathrm{s}$, and stress ~100 GPa during crater formation. For clusters with $\sim 10^3$–10^5 atoms a combination of evaporation and molten flow leads to crater volumes in the linear regime ($a \sim 0.3$, $t_c \sim 10$ ps, $\dot{\epsilon} \sim 10^{12}/\mathrm{s}$, and stress ~50 GPa). For sizes of $\sim 10^5$–10^7 atoms molten flow plays a crucial role, with some contribution from plastic flow ($t_c \sim 50$ ps, $\dot{\epsilon} \sim 10^{11}/\mathrm{s}$, and stress ~5 GPa). For larger sizes, we use the cratering times as estimated in Ref. [17], which represent macroimpacts reasonably well but overestimates cratering times by a factor of ~4 for the largest nanoprojectiles in our simulations. For microscopic sizes, with 10^{10}–10^{13} atoms ($t_c \sim 20$ ns, $\dot{\epsilon} \sim 10^8/\mathrm{s}$, and stress ~1 GPa), and for macroscopic sizes with 10^{20}–10^{25} atoms ($t_c \sim 100$ μs, $\dot{\epsilon} \sim 10^4/\mathrm{s}$, and stress ~0.1 GPa), plastic flow aided by preexisting defects (dislocations, grain boundaries, cracks, etc.) dominates crater formation [1,17]. Figures 2(a) and 2(b) mark the beginning of the transition to the microregime.

Our simulations allow us to obtain insight on how plastic flow helps excavating deeper craters and increasing the cratering efficiency a, since we can directly observe the dislocations formed by the impact and relate the induced plastic flow to the crater volume. Note that in the analysis of macroscopic craters, a ''cratering efficiency'' is often defined as the ratio of the crater volume to the maximum possible crater volume, based on an effective target strength. Then an increase of cratering efficiency is interpreted as being due to a decrease in effective target strength.

It is well known that the strength Y of materials depends on the velocity with which it is deformed, i.e., on the strain rate $\dot{\epsilon}$. This is particularly true at the ultrahigh strain rates produced by nanocluster impact. For instance, the strength of Cu at $\sim 10^4/\mathrm{s}$ is 0.2 GPa, and 1.1 GPa at $\sim 10^{10}/\mathrm{s}$ [18], with a maximum of 2.5 GPa observed in MD simulations at $10^{12}/\mathrm{s}$ [19]. The strength of a material actually depends on both pressure and strain rate, and for shocks, these are related by the Schwegle-Grady (SG) empirical relationship [20]. The strain rates and pressures we obtain directly from our MD results compare well with those from SG extrapolated at higher strain rates.

Stradling *et al.* [17,21] brought up the idea that an increase in strength may be responsible for the size effect in impact-induced crater sizes for the special case of 6 km/s μm- vs mm-sized impacts into Cu, and it was shown that the inclusion of the rate dependence using the Preston-Tonks-Wallace (PTW) strength model [22] allows for a rough fit of the experimental data [23]. However, it cannot explain the factor of ~50 in the scaling parameter a between nano- and macroimpacts. One would need to assume $Y \sim 10$ GPa, well above its maximum ideal value, to account for such differences. As we show below, it is actually a combination of factors which leads to the large change in efficiency, chiefly molten flow and dislocation production and flow, partly driven by the large stress associated with large strength and strain rates.

Recent experiments [18,24] and simulations [19,25] show that the large production of dislocations at the ultrahigh strain rates produced by high-power laser loading lowers the flow stress compared to the one for a material without such high dislocation densities, allowing massive plastic flow. As we can directly observe the formation and propagation of dislocations in our simulation, we can immediately assess the contribution of plastic flow, similarly to the case of dislocations produced by a flat steady piston [19]. Plastic activity increases temperature and facilitates plastic flow.

Orowan's equation [26] states that

$$\epsilon_p = \rho b v t_c, \tag{2}$$

where ρ is the mobile dislocation density, and $b = 0.25$ nm is the Burgers vector in Cu. It relates the plastic strain ϵ_p to the dislocation velocity v and the cratering time t_c available for motion. Note that small projectiles might cause a huge pressure under the impact point, and therefore trigger massive dislocation densities, a few times $10^{13}\ \mathrm{cm}^{-2}$; see also Supplemental Material [16]. However, such densities will be extremely localized and will not lead to dislocation motion beyond very short times and plastic flow will not be as relevant. For larger projectiles, dislocation densities would be lower, but their motion would last for relatively long times, contributing to a larger plastic flow [19,25]. Motion, helped by a longer push from the projectile acting as a shock piston, would continue until an evolved dislocation array with a large number of junctions slows down plastic flow. Such dislocation arrays do survive in our simulation long after the crater evolution has stopped and show a power law decrease with distance from the crater bottom. This is similar to experimental results [27], where electron microscopy shows extensive dislocation networks below macroscopic craters, accompanied by

a power law hardness behavior, where hardness can be taken as being proportional to dislocation density.

Our simulations—here taken for the case of a cluster impacting at ~5 km/s into Cu, with diameter $D = 10$–55 nm—show that the mobile dislocation density is $\rho \sim 10^{12}$–10^{13} cm^{-2}; these dislocations are moving with a high velocity of $v \sim 0.5 v_s$ ($v_s = 4$ km/s is the velocity of sound of Cu). These numbers give a plastic strain of $\epsilon_p \sim 25\%$ during the time of crater formation $t_c \sim$ 5–50 ps. In other words, ~25% of the crater depth and radius, and accordingly ~50% of its volume are due to plastic flow. Using time dependent values of dislocation densities and velocities gives similar results. Melt flow, on the other hand, contributes to 10%–30% of the crater volume for the same cases.

In order to test the general validity of our discussion, we have carried out simulations of model brittle solids, based on the Lennard-Jones interaction potential, and observe the same features as in our ductile Cu simulations [6,28].

Experimental data for the nm cluster sizes (number of atoms $N \lesssim 10^7$ atoms), for which more extensive molecular-dynamics results will be possible in the near future, are now available from measurements of interplanetary dust-particle impacts on spacecraft surfaces as in Fig. 3 [2], and could be obtained by novel laboratory techniques [29]. Our reduced cratering efficiency at small sizes might contribute to the design of better surface nanostructuring and modification techniques [3], change dust and gas phase life cycle estimates for the solar and interstellar medium [30], revise temperature and pressure estimates during crater impact relevant for biomolecule formation [31], help to explain the kink observed in crater frequency at sizes below 200 nm in STARDUST foils [2], and push the development of advanced materials models which work from the nano- to the macroscale in multiscale simulations.

E. B. acknowledges support from PICT2009-0092, from the Argentinean Research Agency. Helpful discussions with J. Samela, K. Nordlund, and T. Aoki are acknowledged. M. Duchaineau created the parallel visualization software which generated Fig. 2, and F. Fioretti carried out simulations with defective samples.

*urbassek@rhrk.uni-kl.de
http://www.physik.uni-kl.de/urbassek/

[1] H. J. Melosh, *Impact Cratering: A Geologic Process* (Oxford UP, New York, 1989).
[2] F. Hörz *et al.*, Science **314**, 1716 (2006).
[3] I. Yamada, J. Matsuo, Z. Insepov, T. Aoki, T. Seki, and N. Toyoda, Nucl. Instrum. Methods Phys. Res., Sect. B **164–165**, 944 (2000).
[4] R. Aderjan and H. M. Urbassek, Nucl. Instrum. Methods Phys. Res., Sect. B **164–165**, 697 (2000).
[5] J. Samela and K. Nordlund, Phys. Rev. Lett. **101**, 027601 (2008).
[6] C. Anders, G. Ziegenhain, S. Zimmermann, and H. M. Urbassek, Nucl. Instrum. Methods Phys. Res., Sect. B **267**, 3122 (2009).
[7] In the simulations, the spherical cluster impacts perpendicular into the solid. The size of the target varies between 10^5 and 10^{10} atoms depending on the size and energy of the cluster. For the larger targets LAMMPS [8] was employed. Damped boundary conditions are used in order to mimic energy dissipation to the surrounding target material. Cu is described by the Mishin potential [9].
[8] http://lammps.sandia.gov/.
[9] Y. Mishin, M. J. Mehl, D. A. Papaconstantopoulos, A. F. Voter, and J. D. Kress, Phys. Rev. B **63**, 224106 (2001).
[10] Another type of nonlinearity occurs at small E/U and small V. It is due to a—rather trivial—threshold phenomenon: at too small impact energies, projectiles do not excavate a crater.
[11] E. Pierazzo, A. M. Vickery, and H. J. Melosh, Icarus **127**, 408 (1997).
[12] M. J. Cintala and R. A. F. Grieve, Meteorit. Planet. Sci. **33**, 889 (1998).
[13] K. Nordlund, J. Keinonen, M. Ghaly, and R. S. Averback, Nucl. Instrum. Methods Phys. Res., Sect. B **148**, 74 (1999).
[14] J. Samela and K. Nordlund, Nucl. Instrum. Methods Phys. Res., Sect. B **267**, 2980 (2009).
[15] T. J. Colla, R. Aderjan, R. Kissel, and H. M. Urbassek, Phys. Rev. B **62**, 8487 (2000).
[16] See Supplemental Material at http://link.aps.org/supplemental/10.1103/PhysRevLett.108.027601 for tabulation of crater volumes, calculation of dislocation densities, cratering times, pressure and strain rates, for differences between ductile vs brittle solids, and defective samples.
[17] J. M. Walsh, G. L. Stradling, G. C. Idzorek, B. P. Shafer, and H. L. Curling, Jr., Int. J. Impact Eng. **14**, 775 (1993).
[18] W. J. Murphy *et al.*, J. Phys. Condens. Matter **22**, 065404 (2010).
[19] E. M. Bringa, K. Rosolankova, R. E. Rudd, B. A. Remington, J. S. Wark, M. Duchaineau, D. H. Kalantar, J. Hawreliak, and J. Belak, Nature Mater. **5**, 805 (2006).
[20] J. W. Swegle and D. E. Grady, J. Appl. Phys. **58**, 692 (1985).
[21] G. L. Stradling, G. C. Idzorek, B. P. Shafer, H. L. Curling, Jr., M. T. Collopy, A. A. H. Blossom, and S. Fuerstenau, Int. J. Impact Eng. **14**, 719 (1993).
[22] D. L. Preston, D. L. Tonks, and D. C. Wallace, J. Appl. Phys. **93**, 211 (2003).
[23] R. F. Davidson and M. L. Walsh, AIP Conf. Proc. **370**, 1159 (1996).
[24] H.-S. Park, K. T. Lorenz, R. M. Cavallo, S. M. Pollaine, S. T. Prisbrey, R. E. Rudd, R. C. Becker, J. V. Bernier, and B. A. Remington, Phys. Rev. Lett. **104**, 135504 (2010).
[25] M. A. Shehadeh, E. M. Bringa, H. M. Zbib, J. M. McNaney, and B. A. Remington, Appl. Phys. Lett. **89**, 171918 (2006).
[26] J. P. Hirth and J. Lothe, *Theory of Dislocations* (Wiley, New York, 1982), 2nd ed.
[27] S. A. Quinones and L. E. Murr, Phys. Status Solidi (a) **166**, 763 (1998).
[28] C. Anders, E. M. Bringa, G. Ziegenhain, and H. M. Urbassek, New J. Phys. **13**, 113019 (2011).

[29] J. F. Hansen, W. van Breugel, E. M. Bringa, B. Eberly, G. A. Graham, B. A. Remington, E. A. Taylor, and A. G. G. M. Tielens, JINST **6**, P05010 (2011).

[30] E. Grün, in *Encyclopedia of the Solar System* (Academic Press, Amsterdam, 2007), p. 621.

[31] Y. Furukawa, T. Sekine, M. Oba, T. Kakegawa, and H. Nakazawa, Nat. Geosci. **2**, 62 (2009).

[32] E. Turtle, E. Pierazzo, G. Collins, G. Osinski, H. Melosh, J. Morgan, and W. Reimold, Geol. Soc. Am. Spec. Pap. **384**, 1 (2005).

[33] L. E. Murr, S. A. Quinones, E. Ferreyra, A. Ayala, O. L. Valerio, F. Hörz, and R. P. Bernhard, Mater. Sci. Eng. A **256**, 166 (1998).

[34] C. A. Wingate, R. F. Stellingwerf, R. F. Davidson, and M. W. Burkett, Int. J. Impact Eng. **14**, 819 (1993).

[35] R. F. Davidson and M. L. Walsh, in *Proceedings of the 1995 APS Topical Conference on Shock Compression of Condensed Matter* (Los Alamos National Laboratory, Los Alamos, NM, 1995), pp. LA–UR–95–2746.